IOPscience iopscience.iop.org

Home Search Collections Journals About Contact us My IOPscience

Quantitative electron holography of biased semiconductor devices

This article has been downloaded from IOPscience. Please scroll down to see the full text article.

2004 J. Phys.: Condens. Matter 16 S181

(http://iopscience.iop.org/0953-8984/16/2/021)

View the table of contents for this issue, or go to the journal homepage for more

Download details:
IP Address: 129.252.86.83
The article was downloaded on 28/05/2010 at 07:16

Please note that terms and conditions apply.

INSTITUTE OF PHYSICS PUBLISHING JOURNAL OF PHYSICS: CONDENSED MATTER

J. Phys.: Condens. Matter **16** (2004) S181–S192 PII: S0953-8984(04)66988-8

Quantitative electron holography of biased semiconductor devices

A C Twitchett, R E Dunin-Borkowski, R F Broom and P A Midgley[1]

Department of Materials Science and Metallurgy, University of Cambridge, Pembroke Street, Cambridge CB2 3QZ, UK

E-mail: pam33@cam.ac.uk

Received 31 July 2003
Published 22 December 2003
Online at stacks.iop.org/JPhysCM/16/S181 (DOI: 10.1088/0953-8984/16/2/021)

Abstract
Off-axis and in-line electron holography have been used to determine the electrical properties of a silicon p–n junction. Specimens were prepared for transmission electron microscopy (TEM) by focused ion beam (FIB) thinning and examined in a biasing holder, with holograms recorded as a function of specimen thickness and applied reverse bias. The data revealed the important role played by the surfaces of the thin TEM sample which affect the electrostatic potential distribution within the specimen. The presence of electrically inactive layers, corresponding to the FIB-damaged amorphous surface and an additional crystalline layer, was inferred from the experimental results. Such effects must be taken into account if electron holography is to be used in a reproducible and quantitative way for the examination of semiconductor devices.

1. Introduction

There is a pressing need in the semiconductor industry for quantitative, high spatial resolution techniques that can be used to examine dopant distributions or electrostatic potentials in semiconductor devices in two or three dimensions. A technique that promises high spatial resolution coupled with true quantitative analysis is electron holography, which was first developed by Gabor [1] for the improvement of resolution in electron microscopy images. Electron holography is essentially a method by which both amplitude and phase information can be reconstructed from an image in which only intensities have been recorded.

In Gabor's original paper, a method that we would now refer to as 'in-line holography' is described. In essence, an out-of-focus image is recorded with coherent illumination. The aberrations of the imaging system act to mix the amplitude and phase information in this image; for example phase information in the exit wavefunction is encoded in the intensity variation of the recorded image. In principle the amplitude and phase information can be recovered directly

[1] Author to whom any correspondence should be addressed.

© 2004 IOP Publishing Ltd Printed in the UK

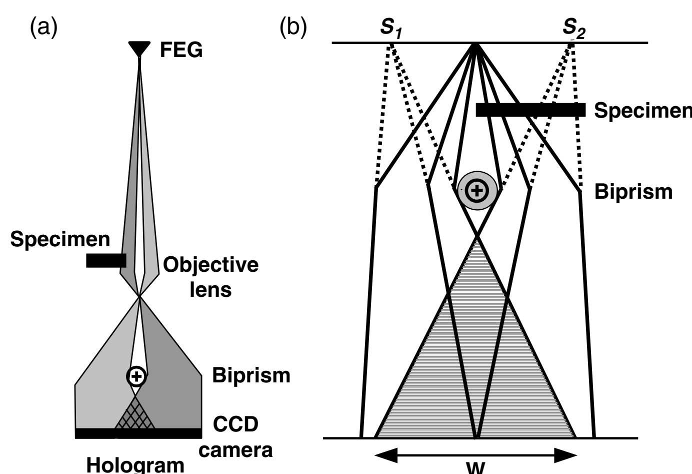

Figure 1. (a) Schematic diagram illustrating off-axis electron holography. The field emission gun (FEG) provides a coherent source of electrons. For acquiring holograms of semiconductor devices the objective lens is replaced with a Lorentz lens to provide an optimal field of view and spatial resolution. A positive voltage is applied to the biprism wire to form the hologram, which is recorded digitally using a charge-coupled-device (CCD) camera. (b) Action of the charged biprism allowing the reference wave to interfere with the wave passing through the sample. A hologram with interference width, W, results from two virtual sources, S_1 and S_2.

from the in-line hologram, or Fresnel image [2], according to Gabor's ideas. However, the reconstructed image is always disturbed by a 'ghost' or 'conjugate' twin image and so in practice phase information is often extracted from in-line holograms by matching simulations to experimental images until a best-fitting model is found. Examples of this approach will be shown below.

For the most part, Gabor's original holography technique has been superseded by 'off-axis holography', which does not suffer from the twin image problem. In the off-axis technique, an electron biprism [3], typically a positively charged gold-coated quartz fibre, acts to bring together two halves of the electron wave, the 'reference' and 'object' waves, giving rise to interference. A hologram is then formed in the image plane, as shown in figure 1(a). If the reference wave has uniform phase, as would be the case in a field-free vacuum, then the reconstructed phase of the hologram can be related directly to that of the object.

The action of the biprism is shown in figure 1(b). From the ray diagram, it is clear that applying a positive potential to the biprism is equivalent to splitting the single electron source into two virtual sources, S_1 and S_2. As with all forms of holography it is essential that coherent illumination is used. In reality the source is never perfectly coherent, either spatially or temporally, but the degree of coherence must be such that an interference pattern of sufficient contrast and intensity can be recorded in a reasonable time to avoid specimen drift and/or beam drift. A field emission gun transmission electron microscopy (TEM) is normally used to provide such a bright coherent source of electrons. To retain high contrast in the interference pattern the wavefront needs to be in phase over the interference width, W.

A hologram can be thought of most simply as an interference pattern in which the carrier fringes have been modulated both in amplitude and in frequency. In order to recover the phase and amplitude changes, the hologram is Fourier transformed to reveal 'sidebands', which are centred at the carrier frequency. When the sideband is selected, either optically or digitally, and back-transformed, the amplitude and phase images are recovered. Normally, a blank

('reference') hologram is also recorded in order to take into account the geometric distortions of the microscope projector lenses [4].

The recorded amplitude is associated with the mass-thickness of the sample, and is similar to an energy-filtered conventional bright-field image. The phase is associated with the presence of an electrostatic or magnetic potential and is initially determined modulo 2π. As a result, the final phase image may show 2π phase jumps. Phase 'unwrapping' removes these jumps, and there are now a number of algorithms to do this accurately and consistently [5].

2. Electron holography of semiconductors

Attempts have been made for over 30 years to use TEM to investigate electrostatic potential distributions arising from dopants in semiconductors [6, 7]. Recently, Rau *et al* [8] used off-axis electron holography to determine the two-dimensional dopant profile in a transistor. The key to the paper's success was the quality of the samples examined. The observed contrast resulted from the fact that under weakly diffracting conditions, for a non-magnetic specimen, the recorded phase ϕ is directly proportional to the electrostatic potential, V, associated with the specimen, i.e.

$$\phi(x, y) = C_E \int V(x, y, z)\, dz \tag{1}$$

where the integral is performed over the electron beam's path and C_E is a known microscope-dependent parameter [4]. In the absence of stray fields and for a uniform potential distribution parallel to the beam in a specimen of thickness, t, this equation can be simplified to

$$\phi(x, y) = C_E V(x, y)t. \tag{2}$$

Rau's work demonstrated vividly the potential of electron holography as a technique for characterizing semiconductor device structures such as p- and n- metal–oxide semiconductor (MOS) transistor structures. This paper noted the presence of electrically 'dead' layers at the sample surfaces, a subject that we will return to below. McCartney *et al* [9], however, examined a silicon p–n junction prepared using tripod polishing and limited ion beam milling and carbon coating, and reported a notable absence of such electrically 'dead' layers on the sample surfaces.

Although the contrast in phase images recorded from doped semiconductors is often qualitatively 'correct', when the magnitude of the built-in potential across a p–n junction is measured from such images, it is often considerably smaller than expected. In order to investigate the origin of such inconsistencies, we have conducted a series of experiments to investigate the effect of the sample surface on the electrostatic potential distribution in a TEM sample. We address, in particular, the effect of focused ion beam (FIB) thinning on the electrical state of the sample surface. This technique is now used routinely to prepare site-specific regions of semiconductor devices for TEM examination. This paper illustrates some of the many issues that must be addressed before electron holography can be used as a fully quantitative characterization technique for the examination of the electrostatic potential in semiconductor devices.

3. Results

In order to ensure consistency and an accurate appraisal of the results, we decided to examine a single well-characterized silicon wafer with a single p–n junction 2.5 μm below the wafer surface. The nominal dopant concentrations were 5×10^{18} cm^{-3} in both the p-type (B-doped)

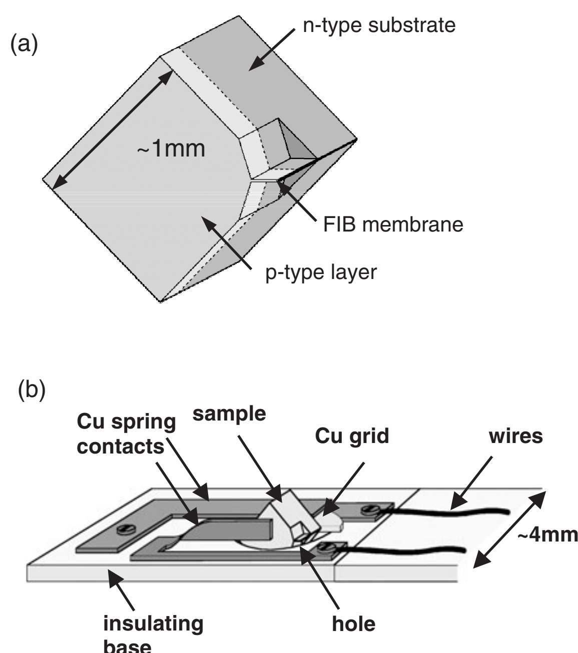

Figure 2. (a) Schematic diagram showing the sample geometry for electrical biasing experiments. The sample is prepared by cleaving a 1 mm square of wafer, one corner of which is subsequently FIB milled parallel to the original wafer growth direction. (b) Schematic diagram of the contact geometry of the electrical biasing holder. The sample is glued to the edge of a Cu grid using conducting epoxy and then clamped between two spring contacts on an insulating base.

and the n-type (Sb-doped) regions. Secondary ion mass spectrometry (SIMS) analysis revealed the true dopant concentrations to be 4×10^{18} cm^{-3} on the p-side and 3×10^{18} cm^{-3} on the n-side. TEM samples containing membranes with four different thicknesses were prepared using a standard trench geometry in an FEI FIB 200 workstation. In addition, we designed and built a biasing holder to allow the p–n junction to be forward or reverse biased *in situ* in the electron microscope [10]. In order to apply a bias, a new specimen geometry was developed. Figure 2(a) shows a schematic diagram of the specimen, which was prepared by initially cleaving a 1 mm square of wafer and then ion milling using the FIB to leave a parallel-sided membrane at the vertex of the cleaved wedge. Additional cuts were milled to provide areas of vacuum close to the region of interest for electron holography. Figure 2(b) shows a schematic diagram of the geometry of the biasing holder.

Off-axis electron holograms of the FIB-prepared membranes were recorded, both with and without an applied electrical bias, using a Philips CM300 FEGTEM operated in ‘Lorentz mode’ with the main objective lens switched off. An objective mini-lens (the Lorentz lens) was used to provide a large field of view of $\sim$1 μm but with a small holographic fringe spacing of $\sim$3 nm. For each hologram, the sample was tilted away from strongly diffracting orientations, to minimise diffraction effects, about an axis perpendicular to the p–n junction, to ensure the junction remained parallel to the beam. Biprism voltages of between 80 and 100 V and applied reverse bias voltages of 0–3 V were used.

A representative phase image reconstructed from an unbiased off-axis electron hologram of the Si p–n junction sample is shown in figure 3. The sample edge is at the lower right of the image. The phase variation in the main part of the specimen has been unwrapped to remove

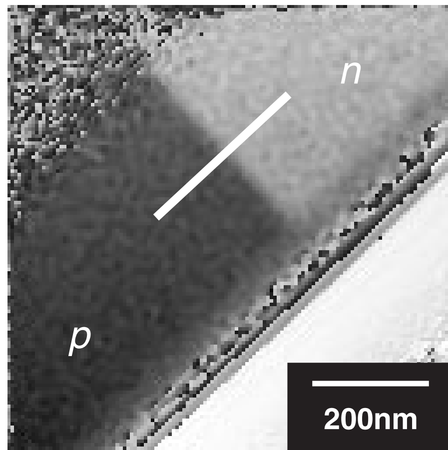

Figure 3. Representative phase image reconstructed from an off-axis electron hologram of a Si p–n junction. No attempt has been made to remove the phase 'wraps' at the sample edge. The white line shows the region from which phase profiles were obtained for figure 6.

the 2π phase jumps. However, no attempt has been made to remove the phase 'wraps' at the sample edge, where the phase change is very rapid. In our specimens which were prepared by FIB there was no evidence of electrostatic fringing fields in the vacuum either before or during biasing: the phase was always completely flat. In contrast, wedge specimens that had been cleaved (with no ion beam thinning) showed significant external variations in the electrostatic potential arising from the reverse-biased p–n junction, as illustrated in figure 4.

The thicknesses of the sample were measured using both convergent beam electron diffraction [11], which revealed the total thickness of crystalline material, and from the amplitude image, A_r, of the reconstructed hologram, which was used to provide the total (crystalline plus amorphous) sample thickness, t, according to the equation [4]

$$t/\lambda_i = -2 \ln A_r. \qquad (3)$$

Figure 5 shows the sample thickness in units of inelastic mean free path, λ_i, measured from several holographic amplitude images and plotted as a function of the crystalline thickness of the sample measured using convergent beam electron diffraction. The gradient of the graph suggests that λ_i (measured from holographic images) = 85 nm for crystalline Si at 200 kV. The intercept suggests that 60 nm of the total sample thickness is amorphous. These measurements assume that the inelastic mean free path is the same in the amorphous and crystalline silicon.

Figure 6 shows line profiles taken across p–n junctions such as that in figure 3 revealing the measured phase shift across the Si p–n junction, plotted as a function of (a) sample thickness for three different unbiased samples, and (b) reverse bias voltage for a single sample of 390 nm crystalline thickness. Figure 6(c) shows the height of the step in phase shift across the junction as a function of applied bias for the same sample. The slope of this graph suggests that the electrically active thickness of the sample is 340 nm, and that an electrically dead crystalline layer is present in addition to the amorphous layers inferred from figure 5.

For comparison, a series of in-line holograms (defocused bright-field images) was acquired from the same samples. For a p–n junction recording an image in focus will yield no contrast but, by defocusing, the potential drop across the junction is revealed by an asymmetric series of black and white fringes. Figure 7 shows a representative image taken from such a defocus series. In order to allow the contrast to be quantified, it is vital that the inelastic background

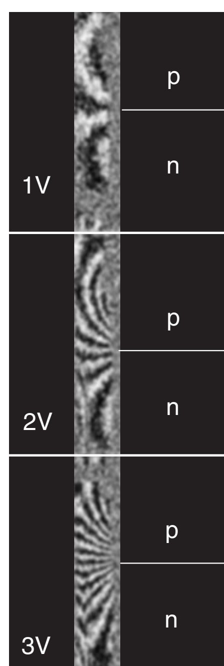

Figure 4. Four times amplified phase images showing the electrostatic fringing field outside a cleaved wedge for 1, 2 and 3 V applied reverse bias. The zero bias hologram was used as the reference hologram in each case to remove any small phase variations arising from contributions other than the electrostatic potential across the p–n junction.

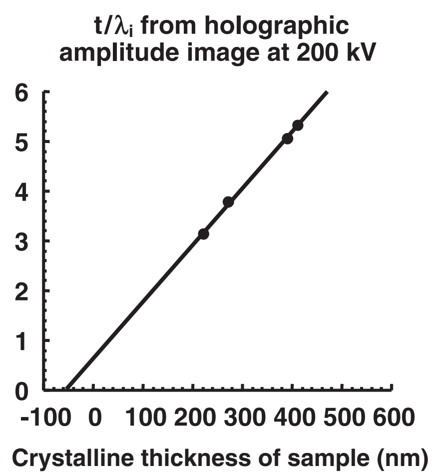

Figure 5. Sample thickness in units of inelastic mean free path measured from holographic amplitude images, λ_i, plotted as a function of the crystalline thickness of the sample, measured using convergent beam electron diffraction. The slope of the graph suggests that $\lambda_i = 85$ nm for crystalline Si at 200 kV. The intercept suggests that 60 nm of the total sample thickness is amorphous.

(which is very substantial in such thick specimens) is removed by energy-filtering. The images were therefore acquired using a 10 eV energy window centred on the zero loss peak.

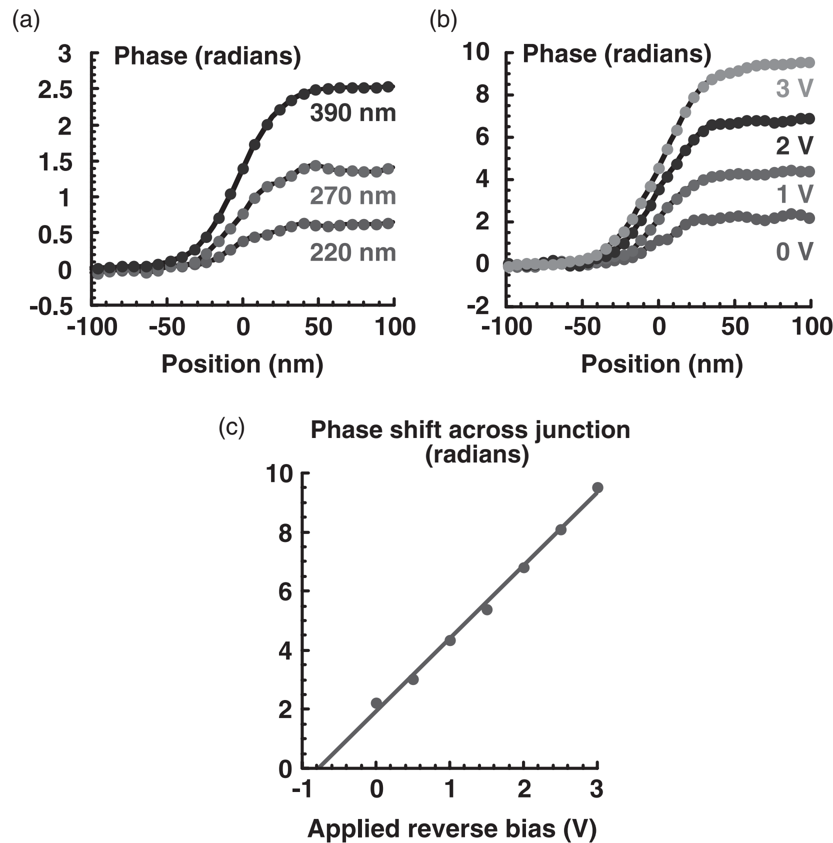

Figure 6. Line profiles showing the measured phase shift across the Si p–n junction, plotted as a function of (a) sample thickness for three different unbiased samples, (b) reverse bias voltage for a single sample of 390 nm crystalline thickness and (c) the total phase shift across the p–n junction as a function of applied reverse bias voltage for the same sample as (b).

In order to obtain the most reliable information from both holographic techniques, simulations were fitted to the phase profiles extracted from the off-axis holograms and to the in-line holograms. For these simulations, a phase grating approximation was found to be sufficient, and a Simplex algorithm [12] was used to iterate the parameters describing the electrostatic potential distribution in the sample. These parameters included the depletion width, the built-in voltage, the electrically active thickness and the ‘abruptness’ of the junction. From the fitted electrostatic potential, the electric field and charge density profiles across the junction were determined using Poisson’s equation. Figure 8 shows fitted electric field and charge density profiles as a function of sample thickness and applied bias. The thickness series cannot be separated easily in figure 8(a), indicating that the electric field across the junction does not change significantly with thickness. From the figures, it is clear that the fitted charge density is lower than predicted and that contrary to expectations, the charge density increases with higher applied voltage. One possible explanation is that the reverse bias is re-activating dopants somehow passivated by sample preparation.

Figure 9(a) shows a representative series of in-line holograms, acquired with defocus values of between -3.5 and $+3.5$ mm and with the microscope operated in Lorentz mode. The absolute defocus values had been pre-calibrated using a catalase specimen for reference.

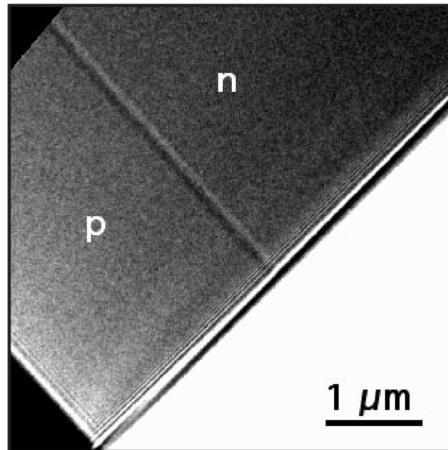

Figure 7. Representative in-line hologram taken at a defocus of +3.5 mm and with an energy filter window of 10 eV centred on the zero-loss peak. The black–white asymmetry reflects the charge density profile.

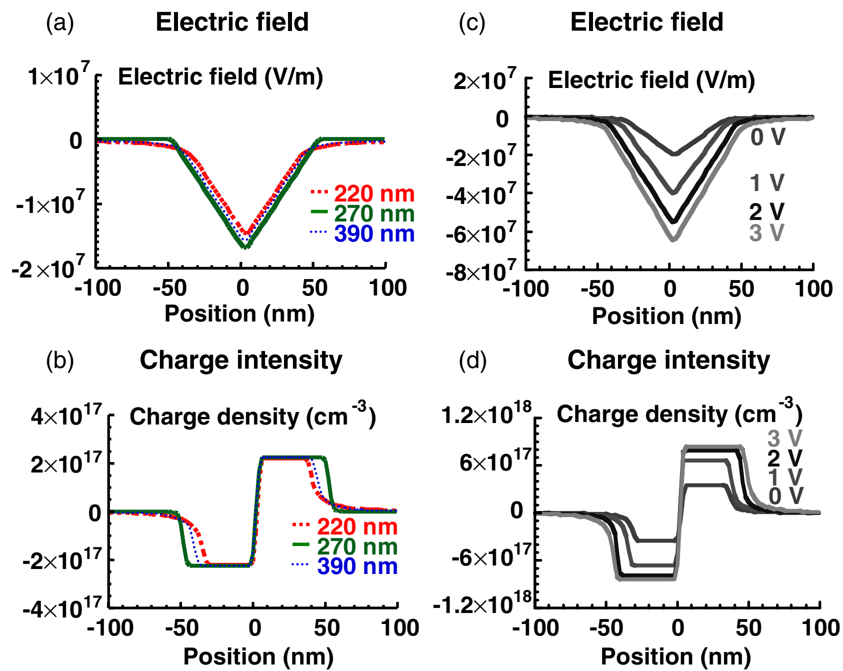

Figure 8. Electric field and charge density profiles generated from best-fitting phase profiles to experimental off-axis data. (a) and (b) show results of the best fit obtained from three unbiased FIB milled samples whose crystalline thicknesses were 220, 270 and 390 nm. (c) and (d) show results as a function of reverse bias voltage from a single FIB-prepared specimen whose measured crystalline thickness was 390 nm.

(This figure is in colour only in the electronic version)

The images contain an asymmetric series of fringes, whose sense reverses with a change in the sign of the defocus. Virtually no contrast is seen at zero defocus, as expected. In the middle

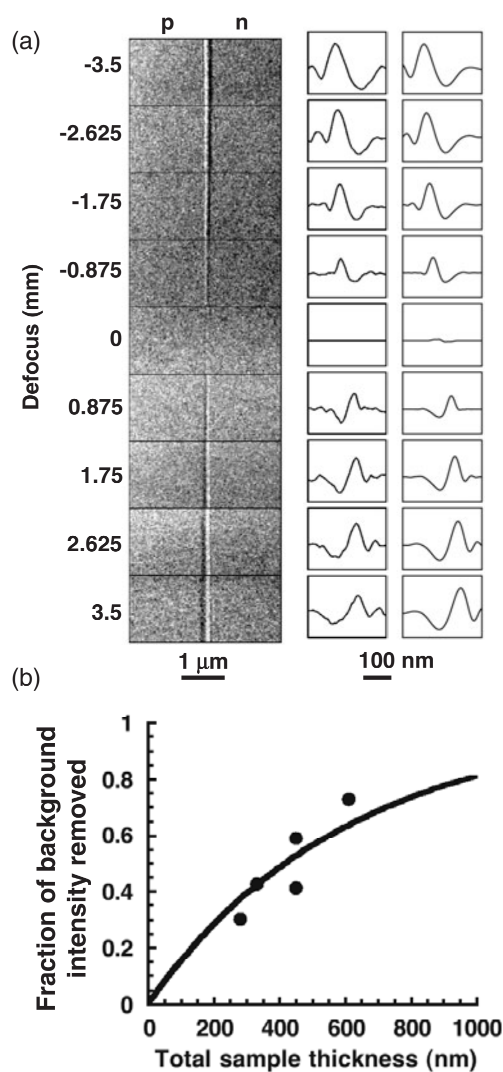

Figure 9. (a) The left-hand column shows a series of in-line holograms as a function of objective lens defocus. The middle column shows extracted line profiles across the junction and in the right-hand column the corresponding best-fitting simulations. (b) shows the fraction of background intensity removed in order to fit the experimental images to the simulations. The curve is a best-fit solution assuming the background arises from diffuse phonon scattering with a mean free path of 600 nm.

of the montage are extracted line profiles across the junction, and to the right are best-fitting simulated profiles. It was found that the recorded experimental in-line data had significantly less contrast than the simulations, and a uniform background had to be removed from the data to provide a match with simulations that was consistent with the potential profiles measured from the same samples using off-axis electron holography. Figure 9(b) shows the fraction of background that had to be removed from the total signal as a function of sample thickness. We postulate that this arises from contributions to the image from incoherent diffuse scattering, and in particular from high angle multiply-scattered phonons. With this idea in mind, a curve

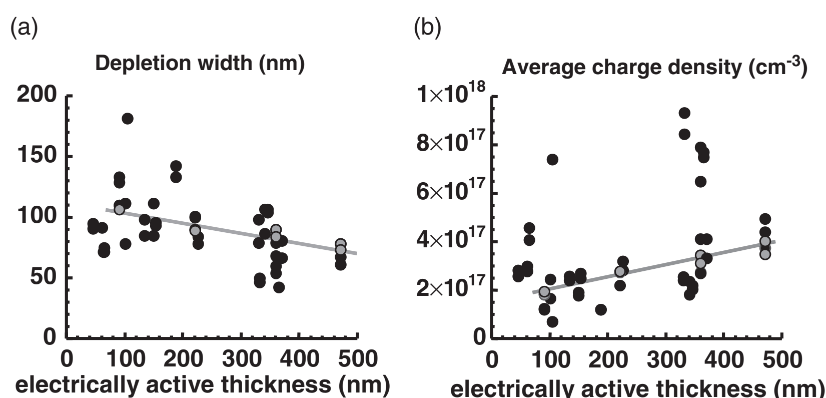

Figure 10. Comparison of (a) minimum depletion widths and (b) charge densities in the depletion region of the Si p–n junction measured using off-axis electron holography (black circles) and in-line holography (grey circles and lines) from a range of unbiased FIB milled samples of different thickness.

of the form $1 - \exp(-t/\lambda)$ was fitted to the data, where t is the sample thickness and λ the phonon mean free path. The best fitting value for λ was 600 nm, which is consistent with published values for the phonon mean free path in Si at 200 kV [13].

It is now possible to look at the results from both sets of holography data derived from the best-fitting potential distributions. Figures 10(a) and (b) show the measured depletion width and charge density plotted as a function of 'electrically active' thickness. In both cases, the black dots correspond to the fitted off-axis holography data and the grey dots and line to the fitted in-line results. The in-line results are consistent with the off-axis data but have less scatter, presumably because of the larger number of data points fitted to the simulations in each defocus series, in which the contrast is both amplified and delocalized from the position of the junction. The in-line data are, in general, more sensitive to the *shape* of the potential well and the off-axis data better at revealing the *magnitude* of the potential step, i.e. the built-in voltage across the junction. However, the measured depletion width and charge density are higher, and lower, respectively, than the predicted values based on the SIMS results. (The expected depletion width for a doping concentration of 1×10^{18} cm^{-3} is 50 nm.) This deviation is almost certainly caused by the sample preparation and we will be addressing this in the future by 'cleaning' thinned samples in various ways.

Our results can be summarised in the form of two figures which are shown in figure 11. These diagrams show the potential distribution schematically for thick and thin TEM specimens, inferred from trends in data acquired at many different sample thicknesses, and outline the significant role played by the sample surfaces. In (a) the majority of the specimen appears to behave in a bulk-like manner. However, near the surfaces the depletion width starts to diverge, so that at the electrically 'dead' amorphous layers the depletion width tends to infinity. The bulk-like semiconductor is effectively sandwiched in between electrically dead crystalline layers, which are themselves sandwiched between electrically dead amorphous (damaged) layers. As the specimen becomes very thin the influence of the surfaces becomes proportionately greater and both the minimum depletion width and the electrically dead crystalline layer become larger. This behaviour is represented in (b). However, the apparent active dopant concentration is still lower than predicted in the bulk-like region, almost certainly arising from a combination of sample preparation and the incident electron beam. In order to obtain a deeper understanding of the factors that affect this behaviour, electrostatic calculations

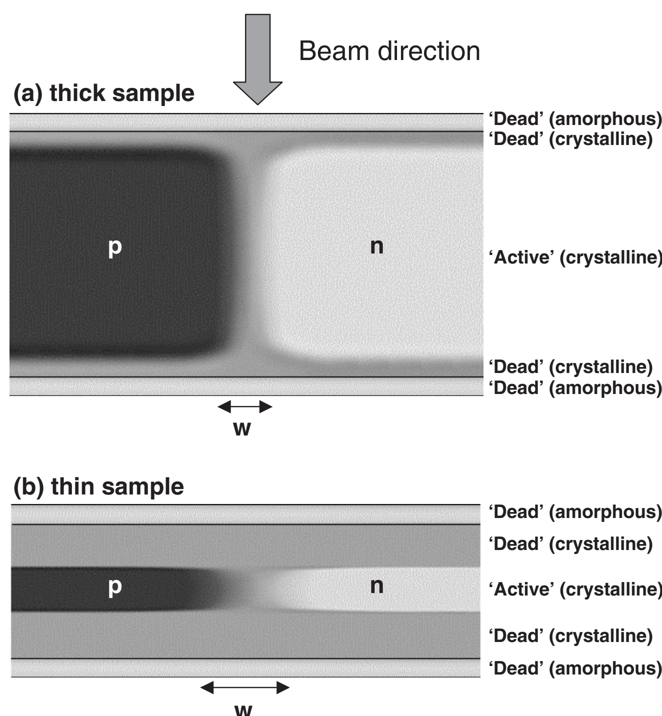

Figure 11. Schematic diagram showing the inferred electrostatic potential and layer structure in cross-section in (a) a thick FIB milled TEM sample and (b) a thin sample.

that take into account the finite dimensions of the specimen and the effect of the incident electron beam on the electrical properties of the sample are required [14, 15].

4. Conclusions

The two-dimensional potential distribution in a thin silicon membrane has been examined using a combination of in-line and off-axis electron holography. The in-line holography results exhibit superior spatial resolution when measuring the potential profile whereas off-axis electron holography provides a better measure of the total potential change across the junction, thus demonstrating the complementary information provided by these two techniques. Electron holography of biased specimens has revealed that the measured active dopant concentration can vary with applied voltage. Such unexpected results require further investigation if electron holography is to be used in a quantitative fashion.

Acknowledgments

The authors would like to thank Mr Robert Hallifax for help in the design and construction of the biasing holder and Dr Rick Hervig at Arizona State University for the SIMS analysis. The authors wish to acknowledge financial support from the Royal Society, the EPSRC and Newnham College, Cambridge.

References

[1] Gabor D 1949 *Proc. R. Soc.* A **197** 454
[2] Ross F M and Stobbs W M 1991 *Phil. Mag.* A **63** 1
[3] Möllenstedt G and Düker H 1956 *Z. Phys.* **145** 377
[4] Midgley P A 2001 *Micron* **32** 167
[5] Ghiglia D C and Pritt M D 1998 *Two-Dimensional Phase Unwrapping* (New York: Wiley)
[6] Titchmarsh J M, Lapworth A J and Booker G R 1969 *Phys. Status Solidi* **34** K83
[7] Matteucci G, Missiroli G F and Pozzi G 2002 *Advances in Imaging and Electron Physics* **122** 183
[8] Rau W D, Schwander P, Baumann F H, Höppner W and Ourmazd A 1999 *Phys. Rev. Lett.* **82** 2614
[9] McCartney M R, Gribelyuk M A, Li J, Ronsheim P, McMurray J S and Smith D J 2002 *Appl. Phys. Lett.* **80** 3213
[10] Twitchett A C, Dunin-Borkowski R E and Midgley P A 2002 *Phys. Rev. Lett.* **88** 238302
[11] Kelly P M, Jostons A, Blake R G and Napier J G 1975 *Phys. Status Solidi* a **31** 771
[12] Press W H, Flannery B P, Teukolsky S A and Vetterling W T 1989 *Numerical Recipes* (Cambridge: Cambridge University Press)
[13] Radi G 1970 *Acta Crystallogr.* A **26** 41
[14] Somodi P K, Dunin-Borkowski R E, Twitchett A C, Barnes C H W and Midgley P A 2003 *Proc. Microscopy of Semiconductor Materials Conf.* at press
[15] Beleggia M, Cardinali G C, Fazzini P F, Merli P G and Pozzi G 2001 *Inst. Phys. Conf. Ser.* **169** 427